Fe^{3+} electron paramagnetic resonance study of a $YCaAlO_4$ single crystal: Study of substitutional disorder

Sushil K. Misra and Serguei I. Andronenko
Physics Department, Concordia University, 1455 de Maisonneuve Boulevard West, Montreal, Quebec, Canada H3G 1M8
(Received 30 May 2001; revised manuscript received 19 September 2001; published 1 March 2002)

X(~9.7 GHz) and *Q*(~35.6) band EPR measurements on a single crystal of Fe^{3+} -doped $YCaAlO_4$ are performed to investigate the effect of substitutional disorder upon introduction of Fe^{3+} ions in this crystal. A model is proposed which takes into account the distribution of the orientations of the magnetic *z* axes of the various Fe^{3+} ions in a Gaussian manner about the *c* axis of the crystal, accounting satisfactorily for the observed angular variation of the Fe^{3+} EPR linewidth due to substitutional disorder. The parameters of this model serve to characterize the disorder. In addition, the Fe^{3+} spin Hamilton parameters were estimated from EPR line positions at 4.2, 77, and 295 K. In particular, the Fe^{3+} zero-field splitting parameter b_2^0 was found to have a rather large value, of ~35 GHz for an inorganic host crystal.

DOI: 10.1103/PhysRevB.65.104435 PACS number(s): 76.30.Fc

I. INTRODUCTION

$YCaAlO_4$ is an interesting crystal, because its structure is similar to that of superconducting oxide materials, such as $La_{2-x}Sr_xCuO_4$, and this material is potentially useful as a solid-state laser[1] owing to the large crystal-field splitting, associated with a rather large zero-field-splitting-(ZFS) parameter b_2^0. Although the Y^{3+} and Ca^{2+} ions substitute at the same crystallographic position in the lattice of $YCaAlO_4$, they possess different charges. This difference in charges leads to a distribution of the crystal field at various Al^{3+} sites, referred to as substitutional disorder hereafter. It is expected to be reflected in the EPR spectrum of the Fe^{3+} impurity ion in this lattice, exhibiting an inhomogeneous broadening of EPR lines. In $YCaAlO_4$, the magnetic axes of the impurity ions should be preferentially oriented along the crystallographic *c* axis.

EPR studies on Ti^{3+}, V^{4+}, and Cr^{3+} ions in $YCaAlO_4$ crystals were carried out by Yamaga and co-workers.[1–4] They exploited the EPR spectra of these ions to investigate substitutional disorder in the $YCaAlO_4$ crystal. For Cr^{3+} they observed five different sets of EPR spectra, due to both ordered (with narrow EPR lines, 5 mT wide) and disordered (with very wide EPR lines, ~45 mT wide) configurations of neighbor Ca and Y ions. Two of these exhibited orthorhombic site symmetry, with the magnetic *z*, *x* and *y* axes being coincident with the [110], $[1\bar{1}0]$, and [001] crystallographic axes, respectively, characterized by two different sets of spin Hamiltonian parameters. The third one, with a relatively very small value of the ZFS parameter, was found to possess a nearly octahedral symmetry. It was concluded that there existed ordered configurations of Ca^{2+} and Y^{3+} ions in these cases, and some of these configurations (shown in Fig. 1) can be related to these three EPR spectra, as discussed by Yamaga *et al.*[4] The remaining two sets of EPR spectra also exhibited an orthorhombic site symmetry, but with the respective magnetic *z* axes being noncoincident with the *c* axis of the crystal, ascribed to disordered configurations of Ca^{2+} and Y^{3+} ions.

In this paper, Fe^{3+} EPR studies are reported on a $YCaAlO_4$ single crystal in the 4.2–295-K range at the *X* band and at 77 and 295 K at the *Q* band. The linewidth data are exploited to study substitutional disorder, while the EPR line positions are used to estimate Fe^{3+} spin-Hamiltonian parameters in $YCaAlO_4$ at 295, 77, and 4.2 K.

II. SAMPLE PREPARATION AND CRYSTAL STRUCTURE

$YCaAlO_4$ single crystals doped with 0.2% and 2% of Fe_2O_3 were grown by the Czochralski technique[1] from melts prepared in iridium crucibles with the compounds $CaCO_3(3N):Y_2O_3(3N):Al_2O_3(3N)=2:1:1$ in an argon gas atmosphere. The pulling and seed-rotation rates used were 0.8–3.0 mm/h and 3–5 rpm, respectively. The resulting ingot was cut and polished into samples with approximate dimensions $1\times1\times1$ mm^3. The cleavage plane is the (001) plane. This fact was used to orient the crystal.

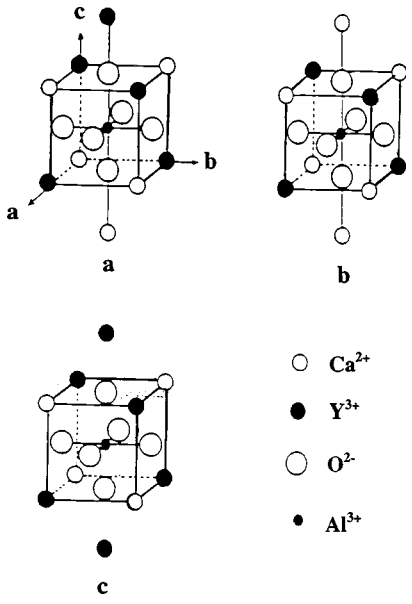

FIG. 1. The ordered configurations of Y^{3+} and Ca^{2+} ions in the structure of $YCaAlO_4$ crystal.

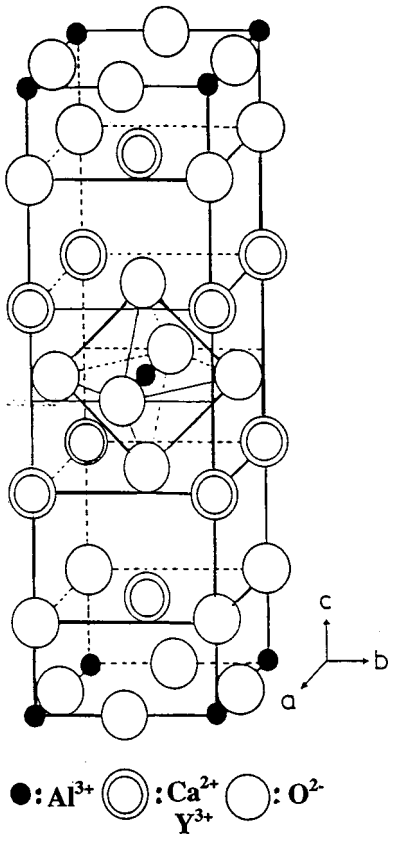

FIG. 2. The unit-cell structure of the $YCaAlO_4$ crystal.

The unit-cell structure of the $YCaAlO_4$ crystal is shown in Fig. 2; it possesses a tetragonal symmetry characterized by the space group $I4/mmm(D_{4h}^{17})$.[1] The unit-cell parameters are $a=b=3.6451$ Å and $c=11.8743$ Å. The distances between the Al^{3+} and O^{2-} ions, located along the *a* and *c* axes, are 1.821 and 1.992 Å, respectively. The point-group (site) symmetry at the Al^{3+} site substituted for by the Fe^{3+} ion, situated at the center of an oxygen tetrahedron, is $4mm$ (tetragonal). Although the Ca^{2+} and Y^{3+} ions have different charges, $+2|e|$ and $+3|e|$, respectively, where $|e|$ is the magnitude of the electron's charge, they occupy the same crystallographic positions in the unit cell, as seen from Fig. 2.

III. EPR SPECTRA

The *Q*- and *X*-band measurements were made on Varian and Bruker spectrometers, respectively; the latter was equipped with an Oxford Instruments helium gas-flow cryostat. The *X*-band measurements were carried out at room (295 K), liquid-nitrogen (77 K), and liquid helium (4.2 K) and in the temperature range 120–300 K, while those at *Q* band were done at 295 and 77 K.

Figures 3–7 show details of EPR spectra in the $YCaAlO_4$ single crystal with 2% Fe^{3+} doping. The room-temperature Fe^{3+} EPR spectra at the *X* and *Q* bands are shown in Fig. 3 for the orientation of the external magnetic field, **B**, along the crystal *c* axis. In Fig. 4 we show the angular variations of the line positions at the *X* band for rotation of **B** in the (110) plane at 295 K; the inset of this figure shows the corresponding angular variation at the *Q* band. In Fig. 5 are shown the angular variations of the line positions for rotation of **B** in the (001) plane; with the inset showing corresponding variation at the *Q* band (35.97 GHz).

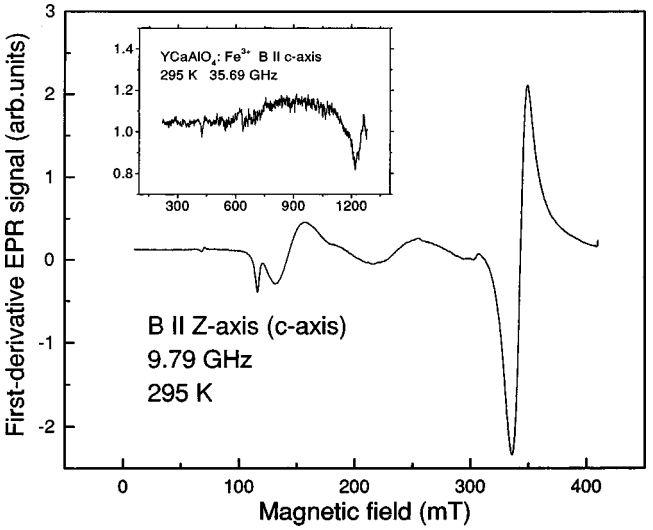

FIG. 3. EPR spectrum of the Fe^{3+} ion in the more concentrated sample with 2% Fe^{3+} doping at 295 K for **B** parallel to the magnetic *z* axis in $YCaAlO_4$ at 9.79 GHz. The inset shows the corresponding spectrum at 35.69 GHz.

$YCaAlO_4$ *crystal with low* Fe^{3+} *doping (0.2%).* There

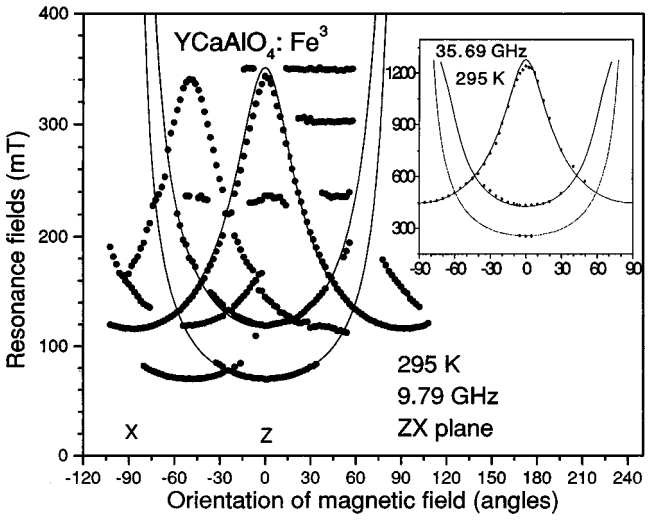

FIG. 4. Simulated and observed (in the more concentrated sample with 2% Fe^{3+} doping) angular variations of Fe^{3+} EPR line positions for Fe^{3+} ions *I* and *II* at 295 K in $YCaAlO_4$ for the orientation of **B** in the magnetic (110) plane, coincident with the magnetic *zx* plane for Fe^{3+} *I* ion, at 9.79 GHz. The inset shows similar plots at 35.69 GHz. The continuous lines represent simulations, while the points represent experimental values. The variations symmetric to the *c* axis represent EPR lines for the Fe^{3+} *I* ion, while those symmetric to $-52°$ represent EPR lines for the Fe^{3+} *II* ion. The glasslike invariant lines at the *X* band observed at about 240, 300, and 350 mT correspond to those Fe^{3+} ions which see random environments about them.

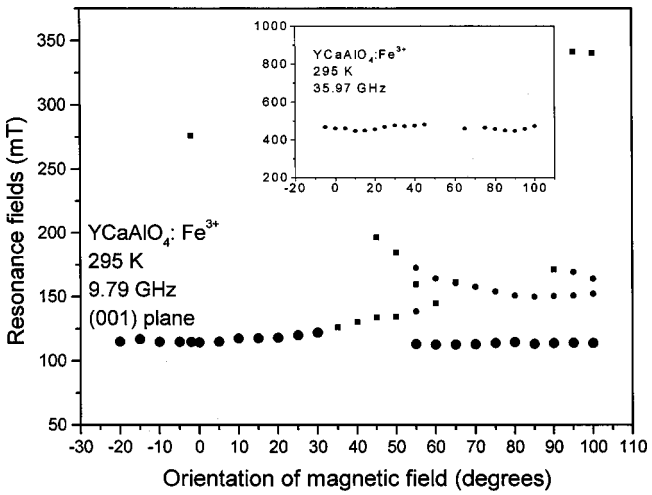

FIG. 5. Observed angular variations of Fe^{3+} EPR line positions at 295 K in $YCaAlO_4$ in the more concentrated sample with 2% Fe^{3+} doping for the orientation of **B** in the magnetic (001) plane, coincident with the magnetic *xy* plane for the Fe^{3+} *I* ion, at 9.79 GHz. The solid circles, insensitive to rotation, show line positions corresponding to the Fe^{3+} *I* ion, while the other line positions correspond to the Fe^{3+} *II* ion. The inset shows the corresponding angular variation at the *Q* band (35.97 GHz).

appears only an EPR spectrum corresponding to the Fe^{3+} *I* ion in this sample. This ion substitutes itself at the Al^{3+} site. This site is easily occupied, since it requires no charge compensation, the ionic radii of these two ions being close to each other: 0.51 Å for Al^{3+} and 0.64 Å for Fe^{3+}. The orientation of the magnetic *z* axis for this ion is expected to be parallel to the *c* axis, consistent with experimental data.

Crystal with 2% Fe^{3+} *doping*. In this sample, there appear

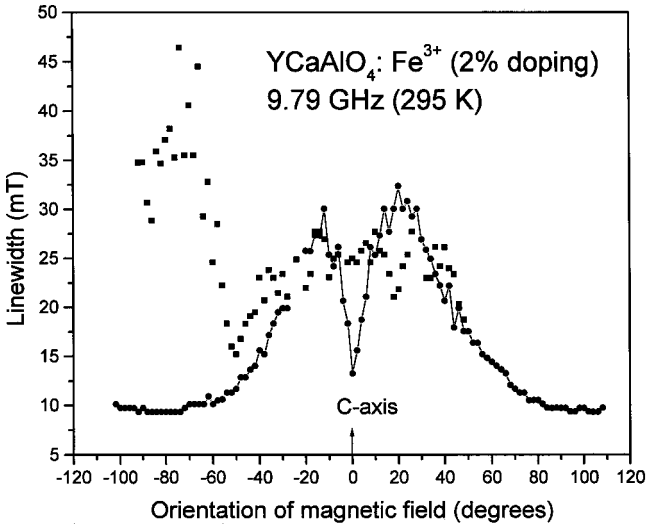

FIG. 6. Observed angular variations of the EPR linewidths for Fe^{3+} *I* and *II* ions at 295 K in $YCaAlO_4$ in a more concentrated sample with 2% Fe^{3+} doping for the orientation of **B** in the magnetic (110) plane at 9.79 GHz. The linewidths corresponding to the Fe^{3+} *I* ion are connected to each other, while the linewidths corresponding to the Fe^{3+} *II* ion are left unconnected.

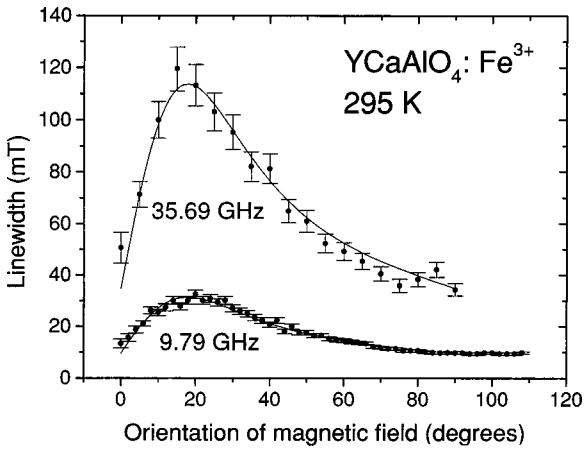

FIG. 7. Observed angular variation of the Fe^{3+} EPR linewidth at 295 K in the magnetic *zx* plane, coincident with the (110) plane, at the *X* band (9.79 GHz) and the *Q* band (35.69 GHz) in the more concentrated sample with 2% Fe^{3+} doping. The continuous lnes show fits to Eq. (6.3), with the parameters given by Eq. (6.4).

three sets of magnetically inequivalent spectra, described as follows.

Sets I and II. These spectra reveal the existence of two magnetically inequivalent Fe^{3+} ions, referred to hereafter as ions *I* and *II*, with the two respective magnetic *z* axes being oriented parallel to the *c* axis and at an angle of $\sim 52°$ from the *c* axis, respectively. (The magnetic *z*, *x* and *y* axes are defined to be those directions of the external magnetic field for which extrema of line positions are observed; of these, the overall splitting of lines are maximum for **B** parallel to the *z* axis and minimum for **B** parallel to the *y* axis).

Set III. It is seen from Fig. 4 that there appear some EPR lines at about 240, 300, and 350 mT, which do not exhibit any angular variation. They can be ascribed to those Fe^{3+} ions, which are characterized by fully disordered arrangement of Y and Ca atoms in their environments, leading to glasslike spectra.

Fe^{3+} *II ion*. Its spectrum appears only in the sample with more concentrated doping (2%) of the Fe^{3+} ions at the *X* band. It is characterized by very wide EPR lines, up to 45 mT in width. Its EPR lines are observed only for a few orientations of **B** with respect to the *c* axis. (At the *Q* band no EPR lines were observed for this ion, as they were completely broadened out.) The crystallographic locations for substitution by Fe^{3+} *II* ions can be deduced as follows by noting the orientation of its magnetic *z* axis. The crystal structure of $YCaAlO_4$ reveals that the line joining an Al^{3+} site with a neighbor Y^{3+} site lies at $\pm 52°$ from the *c* axis in the (110) plane, implying that the Fe^{3+} ion *II* is situated at the Y^{3+} site position, with its magnetic *z* axis pointed toward the site of the adjacent Al^{3+} ion. Now the Y^{3+} ion, with an ionic radius 0.893 Å, is significantly larger than the Fe^{3+} ion with an ionic radius 0.64 Å. For this reason, the Fe^{3+} *II* ion becomes slightly displaced from the regular lattice site occupied by an Y^{3+} ion, resulting in the site symmetry being lower than that it would be if it were situated at the Y^{3+} crystallographic site. Further, it is noted that only one set of EPR spectra for the Fe^{3+} *II* ion, nonsymmetrical with respect

to the *c* axis, was observed, although from structural considerations, there are *expected*, two similar spectra for **B** in the (110) plane for ion *II* with the respective magnetic *z* axes shifted from the *c* axis by $+52°$ and $-52°$, as seen from Fig. 2 showing the unit-cell structure of $YCaAlO_4$. The latter expected EPR spectrum for Fe^{3+} *II* ions was, however, not observed here, implying that only one of the two possible Y^{3+} sites is occupied by Fe^{3+} *II* ions in the sample doped with 2% Fe^{3+} ions.

It may be argued, looking at Fig. 4, that the Fe^{3+} ions *I* and *II* present in the sample, with 2% dopings of Fe^{3+} ions, are physically equivalent if $-26°$ corresponds to the *c* axis, and not 0° as determined here. That this is not true is shown by the following reasons: (i) The *c* axis is really oriented at 0°, since this is an easily identifiable direction being perpendicular to the cleavage, (001), plane. (ii) The angular variation of linewidths for the ions *I* and *II* do not at all show any symmetry with respect to each other, as seen from Fig. 6, showing the angular variation of the linewidths for Fe^{3+} ions *I* and *II* for rotation of **B** in the (110) plane. (iii) The sample with smaller doping (0.2%) of Fe^{3+} ions does not exhibit any lines for the Fe^{3+} *II* ion, and (iv) As discussed above, structural considerations indicate a possible appearance of another symmetrical EPR spectrum for the Fe^{3+} *II* ion, different from that of the Fe^{3+} *I* ion, which was not observed here.

Hereafter, the focus in this paper will be only on an Fe^{3+} *I* ion substituting at the Al^{3+} position, with its magnetic *z* axis being parallel to the crystallographic *c* axis, and its magnetic *zx* plane being coincident with the (110) crystallographic plane which is perpendicular to the cleavage, (001), plane. This ion will be referred to hereafter as an Fe^{3+} ion unless stated otherwise. For this ion, it is found that *not* all expected ''allowed'' transitions ($\Delta M=\pm 1$: $M\leftrightarrow M\pm 1$, where *M* is the electronic magnetic quantum number) were observed, mainly due to the rather large value of the ZFS parameter. Only the EPR transition $-\frac{1}{2}\leftrightarrow\frac{1}{2}$ was observed at all orientations of the magnetic field at both *X*- and *Q*-band frequencies. The other observed transitions were ''forbidden,'' being amongst, the Kramers doublets: $-3/2\leftrightarrow 3/2$ ($\Delta M=\pm 3$) and $-5/2\leftrightarrow 5/2$ ($\Delta M=\pm 5$) transitions. They were, however, observed only over narrow angular ranges for the orientation of **B** due to increased linewidths. Further, no EPR lines for the values of $B>0.35$ T were observed at *X* band, since they were completely broadened out due to increased linewidths. At the *Q* band, no EPR lines for $B>1.3$ T could be observed here, since this was the maximum available magnetic field.

IV. SPIN HAMILTONIAN PARAMETERS

The following spin Hamiltonian (SH) appropriate to tetragonal symmetry was used to fit the EPR line positions to evaluate the SH parameters (SHP's):

$$H=\mu_B[g_{\parallel}B_zS_z+g_{\perp}(B_xS_x+B_yS_y)]+\sum_{n=2,4}^{m=0,4}B_n^mO_n^m. \tag{4.1}$$

In Eq. (4.1), $0\leqslant m\leqslant n$, $S=\frac{5}{2}$ is the electronic spin of the Fe^{3+} ion, μ_B is the Bohr magneton, B_n^m are the SHP parameters, and O_n^m are the Stevens spin operators.[5] Figure 5 is consistent with the tetragonal symmetry ''seen'' by the Fe^{3+} ion *I*, since the lines corresponding to this ion show predominantly axial symmetry perpendicular to the *z* axis, coincident with the *c* axis, for the rotation of **B** in the (001) plane; the fourfold symmetry dictated by the O_4^4 term in Eq. (4.1) is not clearly seen here, presumably due to the rather negligible value of the parameter B_4^4.

There are two aspects to be considered in the determination of SHP's from the EPR line positions in this crystal. First, the EPR line positions are not available for magnetic-field values higher than 0.35 T at the *X* band. Second, due to the rather large Fe^{3+} ZFS parameter ($b_2^0\sim 30$ GHz), there result three well-separated kramers doublets $M=\pm\frac{5}{2}$, $M=\pm\frac{3}{2}$, and ($M=\pm\frac{1}{2}$), within which EPR transitions occur, only the transition within the $\pm\frac{1}{2}$ doublet being allowed. On the other hand, the observation of forbidden EPR transitions within the $\pm\frac{3}{2}$ and $\pm\frac{5}{2}$ doublets become possible due to a mixing of wave functions by the spin Hamiltonian $b_4^4O_4^4$ term, including the operators S_+^4 and S_-^4.[5] (Here $S_{\pm}=S_x\pm iS_y$ are the electron spin raising/lowering operators.)

Since full angular variation was here observed only for the $+\frac{1}{2}\leftrightarrow-\frac{1}{2}$ transition, its EPR line positions for the orientation of **B** away from the *z* magnetic axis were used to estimate b_2^0. This is because the dependence of this line on b_2^0 manifests itself in second order in perturbation theory for orientations of **B** away from the *z* axis, due to the transformation of the spin operators.[5] This dependence reaches a maximum for an orientation of **B** perpendicular to the *z* axis. Specifically, according to perturbation calculations of Ref. 6 quoted by Henderson *et al.*,[7] the effective *g* value for the $+\frac{1}{2}\leftrightarrow-\frac{1}{2}$ transition can be expressed as

$$g(\text{eff})=\{g_{\parallel}^2+(9g_{\perp}^2-g_{\parallel}^2)\sin^2\theta\}^{1/2}\left\{1-2\frac{g_{\perp}\mu_BB}{(2b_2^0)^2}F(\theta)\right\}, \tag{4.2}$$

where

$$F(\theta)=\sin^2\theta\frac{(9g_{\perp}^2\sin^2\theta-2g_{\parallel}\cos^2\theta)}{(9g_{\perp}^2\sin^2\theta+g_{\parallel}^2\cos^2\theta)}. \tag{4.3}$$

If there also exist fourth-order parameters, then $2b_2^0$ in Eq. (4.2) should be replaced by $(2b_2^0-b_4^4-10b_4^0/3)$.[6,7] [Note that the parameters $a=(\frac{2}{5})b_4^4$ and $F=2b_4^0$,[5] where *a* and *F* are the parameters used by Henderson *et al.*[7]) In Eq. (4.2), $g_{\parallel}$ ($=1.991$) and $g_{\perp}$ ($=2.021$) are the *g* values for the Fe^{3+} ion in $YCaAlO_4$, as given in Table I; θ is the angle between **B** and the *z* axis. Then the values of $F(\theta)$, expressing the contribution of b_2^0 to the $+\frac{1}{2}\leftrightarrow-\frac{1}{2}$ transition line position, are 0 and 1 for **B** being parallel to the *z* and *x* axes, respectively, indicating that this transition becomes more and more sensitive to b_2^0 as **B** is rotated away from the *z* axis toward the $x(y)$ axis.

The particular dependence of the $+\frac{1}{2}\leftrightarrow-\frac{1}{2}$ transition line positions on b_2^0 for various orientations of **B** in the *zx* plane,

TABLE I. Spin Hamiltonian parameters for the Fe^{3+} I ion in $YCaAlO_4$ single crystal. The $b_2^0(\equiv 3B_2^0 = D)$ values are in GHz, while the g values are dimensionless. Here sample $(GHz^2) = \Sigma_i(\Delta E_i^{cal}/h - \nu_i)^2/\sigma_i^2$; $\sigma_i = [0.1 + \cos(\theta)]$ and $\sigma_i = 3[0.1 + \cos(\theta)]$ for each data point at 9.79 and 35.69 GHz, respectively. Here θ is the angle between **B** and the z axis, coincident with the c axis. The extra factor 3 in σ_i at the Q band takes into account the increased linewidth from that at the X band. A total of 263 lines at room temperature (199 lines at 9.79 GHz and 64 lines at 35.69 GHz) were simultaneously fitted for the various orientations of the external magnetic field in the zx and xy magnetic planes of the Fe^{3+} I ion. RMSL $(GHz) \equiv (SMD/n)^{1/2}$, where n is the number of lines simultaneously fitted, represents the mean deviation per calculated line from the microwave frequency. Only X-band data were available at 4.2 K.

Frequency (GHz)	Temperature (K)	$g_\parallel$	$g_\perp$	b_2^0	RMSL
9.79+35.69	295	1.991±0.018	2.021±0.006	34.7±0.7	0.28
9.61+35.69	77	1.980±0.023	2.026±0.012	35.4±1.1	0.31
9.61	4.2	2.00±0.05	2.00±0.05	36.0±2.0	0.79

as exhibited by the $g(\text{eff})$ value given by Eq. (4.2), can be exploited to a better determination of b_2^0. This is accomplished by significantly increasing the contribution of line positions to the χ^2 value in the determination of the spin Hamiltonian parameters as the orientation of **B** is rotated from the z axis toward the $x(y)$ axis. Accordingly, the following orientation-dependent factor $\sigma_i(\theta)$ was used in the χ^2 value:

$$\sigma_i(\theta) = p[0.1 + \cos(\theta)], \tag{4.4}$$

where $p = 1.0$, 3.0 for X and Q bands, respectively, taking into account the relative linewidths at the two bands.

The χ^2 value here is defined as

$$\chi^2 = \sum_i (\Delta E_i/h - \nu_i)^2/\sigma_i(\theta)^2. \tag{4.5}$$

In Eq. (4.3), ΔE_i is the calculated energy difference between the levels participating in the resonance, h is Planck's constant, and ν_i is the frequency of the klystron for the ith transition line. It is seen that the weight factor $1/\sigma_i(\theta)^2$, measuring the relative contribution of the various line positions to the χ^2 value, increases from about unity to 100 as **B** approaches the x (y) axis from the z axis. The SHP's $g_\parallel$, $g_\perp$, and b_2^0 for an Fe^{3+} ion in a single crystal of $YCaAlO_4$ were estimated at 295 and 77 K from a simultaneous fitting of the EPR line positions observed at several orientations of **B**, using a least-squares-fitting procedure,[5] with the orientation-dependent χ^2 value defined above by Eq. (4.5), in conjunction with matrix diagonalization. Further, the line positions observed at 9.79 and 35.69 GHz were fitted simultaneously at 295 and 77 K. At 4.2 K, EPR data could only be observed at the X band, since our Q-band spectrometer is not equipped with a liquid-helium temperature accessory.

The resulting values of SHP's are listed in Table I. The fourth-order parameters b_4^m could not be determined precisely due to large linewidths. Based on these SHP's, the angular variations of line positions were simulated at 9.79 and 35.69 GHz. These are also shown in Fig. 4.

V. EFFECT OF DISORDER ON THE EPR LINEWIDTH

There exists disorder in the orientation of the z axes of the various Fe^{3+} ions about the c axis in $YCaAlO_4$, due to distribution of Ca and Y ions in the lattice, which possess different charges although they are situated at the same crystallographic position. As a result, there occurs a distribution of the magnetic z axes of the various FeO_6 complexes about the c axis. This leads to an inhomogeneous broadening of EPR lines, since EPR transitions for differently oriented Fe^{3+} ions occur at different magnetic-field values for a given orientation of **B**. Further, the distribution of the Ca and Y ions, the so-called ''apical'' ions, which lie on the c axis above and below the Fe^{3+} ions, leads to three values of b_2^0, somewhat different from each other, corresponding to three different relative configurations of these two apical ions: Ca-Ca, Y-Y and Ca-Y (Y-Ca). This leads to additional broadening, as well as to slightly asymmetrical shape of EPR lines for the orientation of **B** along the magnetic z axis, as seen from Fig. 3.

VI. A MODEL FOR THE ORIENTATIONAL DEPENDENCE OF THE EPR LINEWIDTH

A model is proposed here to account for the observed angular variation of the EPR linewidth ΔB_{pp}, as shown in Fig. 6, characterized by a maximum at $\sim 20°$ from the c axis at both X and Q bands. The model is based on the fact that the linewidth is due mainly to the angular dependence of the line position on the orientation of **B** with respect to the z axis, and there exists a distribution of the orientations of the magnetic z axes of the various Fe^{3+} ions in the crystal about the c-axis. The details are as follows.

The observed angular variation of the Fe^{3+} EPR resonance line for the $-\frac{1}{2} \leftrightarrow +\frac{1}{2}$ transition of an Fe^{3+} ion, as shown in Fig. 4, can be considered to be due to an effective spin $S = \frac{1}{2}$:

$$B_r(\theta, \theta_1) = \frac{h\nu}{\mu_B \sqrt{g_x^2 \sin^2(\theta_1 - \theta) + g_z^2 \cos^2(\theta_1 - \theta)}}. \tag{6.1}$$

In Eq. (6.1), θ and θ_1 are the angles made by the magnetic z axis of the Fe^{3+} ion under consideration with respect to **B** and the c axis, respectively; thus $(\theta_1 - \theta)$ is the angle between **B** and the c axis. g_z $(= g_\parallel = 2.0)$ and g_x $(= g_\perp = 6.0)$ are the observed g values of the $-\frac{1}{2} \leftrightarrow +\frac{1}{2}$ transition, parallel and perpendicular to the crystallographic c axis (Fig. 4), the

crystallographic *c* axis being parallel to the average orientation of the various magnetic *z* axes as found here from the angular variation of EPR line positions.

It is noted that a similar analysis of the $-\frac{1}{2}\leftrightarrow+\frac{1}{2}$ transition in terms of an effective *g* value for the Fe^{3+} ion in MgO was made by Henderson *et al.*,[7] g(eff), given by Eq. (4.2), using the perturbation expressions derived in Ref. 6, taking into account the effect of the zero-field splitting parameter b_2^0. Their expression [Eq. (4.2)], is consistent with that given by Eq. (6.1) if the b_2^0-dependent term in curly brackets is replaced by 1. This approximation is justified here owing to the rather large value of b_2^0 which leads to $2(g_\perp \mu_B B/2b_2^0)^2 \sim 1/25$.

Now the linewidth is expected to be proportional to the angular derivative $dB_r(\theta,\theta_1)/d\theta$ as a function of the orientation of **B**, because the larger this derivatives the larger the shift of the EPR line position with a variation of **B** with respect to the magnetic *z* axis for a given Fe^{3+} ion. Specifically, from Eq. (6.1) one obtains.

$$\frac{dB_r(\theta,\theta_1)}{d\theta} = -\frac{h\nu}{2\mu_B}\frac{(g_x^2-g_z^2)\sin[2(\theta_1-\theta)]}{[g_z^2\sin^2(\theta_1-\theta)+g_x^2\cos^2(\theta_1-\theta)]^{3/2}}. \tag{6.2}$$

If one now also takes into account the distribution of the magnetic *z* axes of the orientations of the various Fe^{3+} ions about the *c* axis over a small range $\pm\alpha°$ about the *c* axis, assuming a Gaussian distribution, proportional to $\exp[-(\theta_1/\sigma_1)^2]$, the observed EPR linewidth can be expressed, by integrating over the various orientations, as:

$$\Delta B_{pp}(\theta) = A + C\int_{-\alpha}^{\alpha}\frac{dB_r(\theta,\theta_1)}{d\theta}\exp[-(\theta_1/\sigma_1)^2]d\theta_1. \tag{6.3}$$

In Eq. (6.3), *A* is the background linewidth, representing the distribution-independent part of the linewidth. As seen below, it depends linearly on ν, the klystron frequency. As long as α is not too large, such a model based on overlap of lines due to various distributed Fe^{3+} *z* axes is valid.

The expression for ΔB_{pp}, as given by Eq. (6.3), was fitted using Newton's method[8] to the experimentally observed linewidths for the $-\frac{1}{2}\leftrightarrow\frac{1}{2}$ transition for various orientations of **B** separately at 9.7 and 35.6 GHz. The following parameters were obtained:

$$\begin{aligned} &A=9.57\ \text{mT},\quad C=0.0015,\quad \sigma_1=12.7°,\\ &\alpha=24.7°\quad \text{at the } X \text{ band}\\ &A=35.0\ \text{mT},\quad C=0.0020,\quad \sigma_1=9.5°,\\ &\alpha=28.2°\quad \text{at the } Q \text{ band} \end{aligned} \tag{6.4}$$

As a result of fitting, the background linewidth *A* is found to be proportional to the frequency. This is consistent with the experimental data, since as seen from Eq. (6.3), the linewidth is equal to *A* at $\theta=0°$, because the integral in Eq. (6.3) is zero for this value of θ.

It is seen from the values in Eq. (6.4) that the parameters **B** and σ_1 are found to be the same at *X*-and *Q*-band frequencies, within experimental error. From the closeness of the values of *C*, σ_1, and α for the two bands, as given by Eqs. (6.4), and the respective values of *A* being in proportion to klystron frequency, it is tempting to fit simultaneously the observed linewidth at *X* and *Q* bands to the same set of parameters. This yields the following values of the parameters:

$$A=0.9795\nu\ \text{mT},\quad C=0.0018,\quad \sigma_1=11.3°,\quad \alpha=25.2°, \tag{6.5}$$

where ν is the klystron frequency in GHz: 9.79 GHz for the *X* band and 35.69 GHz for the *Q* band.

The angular variation of the observed Fe^{3+} EPR linewidths for the $-\frac{1}{2}\leftrightarrow\frac{1}{2}$ transition at *X* and *Q* bands, as functions of the angle between the *c* axis of the crystal and **B**, are shown in Fig. 7 together with the simulated linewidths calculated using the values given by Eq. (6.5). It is seen from this figure that the simulated linewidth correctly account for the shape of angular variation and occurrence of the maximum of the EPR linewidth at $\theta\sim20°$, as well as the dependence of linewidths on the klystron frequency ν. In particular, it is seen from Eqs. (6.3) and (6.2), in the light of the two sets of data being described by the same values of σ_1 and α, that the observed linewidth at any orientation of **B** is, indeed, proportional to klystron frequency.

Physical situation of the substitutional disorder. On the average, the *z* axes of the various Fe^3 ions in the $YCaAlO_4$ single crystal are distributed about the *c* axis over an angular width $\pm25°$ in a Gaussian manner, with the Gaussian width being about 11°. This describes the disorder of the Fe^{3+} *z* axes superimposed over the regular arrangement of the Fe^{3+} ions at the regular lattice sites substituting for the Al^{3+} ions. This produces an angular variation of the linewidth over and above a constant background dependent upon the klystron frequency (ν GHz) equal to 0.98 ν. Together, all these factors lead to occurrences of maxima in the EPR linewidth for Fe^{3+} *I* ion for orientations of **B** at about $\pm20°$ from the *c* axis.

VII. CONCLUDING REMARKS

The Fe^{3+} EPR linewidth data in $YCaAlO_4$ obtained here have been exploited to (i) estimate spin-Hamiltonian parameters at 295, 77, and 4.2 K using the line positions; and (ii) to study the substitutional disorder in the orientations of the magnetic *z* axes of the various Fe^{3+} ions in $YCaAlO_4$.

Regarding the linewidth, a model has here been developed based on the disorder of Fe^{3+} magnetic *z* axes that accounts satisfactorily for the observed angular variation of the Fe^{3+} EPR linewidth with the orientation of the magnetic field.

As for SHP's, it is found that the value of the zero-field parameter b_2^0 is rather large for an inorganic host crystal, $\approx$30–35 GHz, at various temperatures. Its value was estimated, in the absence of other $\Delta M=\pm1$ transitions whose line positions depend on the parameter b_2^0 in the zero order of perturbation, from the $-\frac{1}{2}\leftrightarrow\frac{1}{2}$ transition line position,

whose value depends on b_2^0 only in second order of perturbation. Higher-frequency (>50 GHz) EPR studies might be helpful for a more complete study due to the very large ZFS characterizing the Fe^{3+} ion in $YCaAlO_4$. However, the increase in linewidth at higher frequencies due to orientational disorder and *g*-anisotropy/strain could be an impediment if the lines become too broad to be observed. An important aspect of this study is the use of the EPR technique to study disorder in host crystals.

ACKNOWLEDGMENTS

The authors are grateful to the Natural Sciences and Engineering Research Council of Canada for partial financial support.

[1] M. Yamaga, P. I. Macfarlane, K. Holliday, B. Henderson, N. Kodama, and Y. Inoue, J. Phys.: Condens. Matter **8**, 3487 (1996).

[2] M. Yamaga, T. Yosida, Y. Naitoh, and N. Kodama, J. Phys.: Condens. Matter **6**, 4381 (1994).

[3] M. Yamaga, B. Henderson, T. Yosida, N. Kodama, and Y. Inoue, Phys. Rev. B **51**, 3438 (1995).

[4] M. Yamaga, T. Yosida, M. Fukui, H. Takeuchi, N. Kodama, Y. Inoue, B. Henderson, K. Holliday, and P. I. Macfarlan, J. Phys.: Condens. Matter **8**, 10 633 (1996).

[5] S. K. Misra, in *Handbook of Electron Spin Resonance*, edited by C. P. Poole, Jr. and H. A. Farach, (AIP, New York, 1999), Chap. VII, p. 115.

[6] E. S. Kirkpatrick, K. A. Müller, and R. S. Rubins, Phys. Rev. **135**, A86 (1964).

[7] B. Henderson, J. E. Wertz, T. P. P. Hall, and R. D. Dowsing, J. Phys. C **4**, 107 (1971).

[8] *Numerical Recipes*, edited by W. H. Press, S. A. Teukolsky, W. T. Vetterling, and B. P. Flannery (Cambridge University Press, New York, 1992), p. 375.